PHOTOCHEMISTRY

Accelerated photochemical reactions at oil-water interface exploiting melting point depression

Ya-Ming Tian, Wagner Silva, Ruth M. Gschwind, Burkhard König*

Water can accelerate a variety of organic reactions far beyond the rates observed in classical organic solvents. However, using pure water as a solvent introduces solubility constraints that have limited the applicability of efficient photochemistry in particular. We report here the formation of aggregates between pairs of arenes, heteroarenes, enamines, or esters with different electron affinities in an aqueous medium, leading to an oil-water phase boundary through substrate melting point depression. The active hydrogen atoms in the reactants engage in hydrogen bonds with water, thereby accelerating photochemical reactions. This methodology realizes appealingly simple conditions for aqueous coupling reactions of complex solid molecules, including complex drug molecules that are poorly soluble in water.

Water, the universal solvent for biochemical transformations, facilitates substrate binding within enzymes, membrane and vesicle formation, and drug incorporation into receptors driven by hydrophobic properties. By contrast, organic chemists have traditionally avoided water as a reaction medium because of limited solubility or sensitivity to hydrolysis of reactants. Nonetheless, groundbreaking research by the Breslow group in 1980 revealed that water can significantly accelerate Diels-Alder reactions involving nonpolar compounds, surpassing the performance of classical organic solvents (*1*). In some cases, reaction rates were enhanced by up to 200-fold. Since then, the assumption that organic reactions necessitate organic solvents for dissolving reactants has been challenged, leading to the exploration of aqueous media for organic transformations. Subsequent studies have demonstrated that aqueous environments can offer faster reaction rates and improved selectivities compared with organic solvents (*2*–*10*). A major milestone in the advancement of aqueous organic synthesis was achieved in 2005, when Sharpless and co-workers reported a series of organic transformations that exhibited accelerated rates when pure water was used as the sole reaction medium, surpassing the performance of nonpolar and polar organic solvents (*11*). Subsequent experimental and theoretical investigations on reactions in aqueous media confirmed the specific properties of water in accelerating organic reactions. These properties include the hydrophobic effect, conventional H bonding, *trans*-H bonding, and others, which exert differential effects on reaction progress under the distinct conditions of "in water" and "on water" (*12*–*22*).

Photochemistry has become a pivotal methodology in advancing organic synthesis (*23*–*28*). However, the use of pure water as a solvent for photochemical transformations has received limited attention to date. Although some applications of photo-induced transformations in aqueous media have started to emerge (*29*–*36*), these reactions have not fully explored the potential of water in accelerating organic transformations compared with commonly used organic solvents. The limitation can be attributed to the complex reaction conditions involving transition metals, the use of cosolvents, the presence of various catalysts, and other factors (*23*, *37*–*45*). Electron donor-acceptor (EDA) photochemistry (*46*, *47*) does not rely on the presence of exogenous photosensitizers. Instead, it focuses on the aggregation between molecules with different electron affinities, which coincides with the fact that water can lead to the acceleration of organic reactions by forcing the formation of aggregates between substrates (*1*–*5*). This strategy offers straightforward reaction conditions and leverages the potential of water to facilitate organic transformations. The synergistic combination of photochemistry and water holds tremendous potential for advancements in the synthesis of pharmaceuticals or materials and in improving sustainability. However, the field remains nascent, offering substantial untapped opportunities for exploration and breakthroughs.

Combining the melting point depression of solid mixtures and hydrophobically enforced substrate aggregation leads to the formation of an oil film on the water surface. These conditions of a well-spread, thin organic liquid film expedite photochemical reactions at the water interface (Fig. 1). Leaving groups such as C(sp^2)–CN, C(sp^2)–F, C(sp^2)–Cl, C(sp^2)–Br, C(sp^2)–SO_2CH_3, and C(sp^3)–Cl are potentially activated by H bonds, and photoinduced electron transfer facilitates their substitution, forming new C(sp^2)–N, C(sp^2)–O, C(sp^2)–S, C(sp^2)–Se, and C(sp^3)–C(sp^2) bonds (there are >160 examples of these). Such cross-coupling reactions usually require conditions in organic solvents using transition metals and/or photocatalysts and additives. We demonstrate the potential of the "on water" photochemical approach in cross- and homocoupling reactions, [2+2] cycloaddition, and the modification of drug molecules. Gram-scale reactions are possible using "on water" photochemistry in flow synthesis.

Synthesis

We began our investigation with indole (**a1**) and isoquinoline-1-carbonitrile (**b1**) as model substrates (see table S1 for model substrate selection details). Under 365 nm light irradiation at 25°C, water facilitated the formation of the N–H arylation product **c1** with a substantial yield of 92% (table S1, entry 1). After evaluating various solvents (Fig. 2A and table S2), we observed that water was superior in promoting the reaction compared with organic solvents. The introduction of methanol in different proportions to water resulted in diminished reaction efficiency, demonstrating a positive correlation between water content and yield. When solid compounds **a1** and **b1** were mixed, the resulting eutectic liquid showed a notably decreased product yield when reacted in neat conditions compared with conditions spread on water. Reaction monitoring for **a1** and **b1** under different solvent conditions (Fig. 2B) showed the acceleration effect of water clearly. The disparity in yield between water as a reaction medium and neat conditions increased over time, whereas the organic solvent acetonitrile showed a much lower initial reaction rate than the conditions in which water was used as a medium from the beginning. We observed that irradiation with longer wavelengths led to a decreased yield because of the reduced absorption ability of the reaction system (table S3). No product was detected in the dark at either 25 or 60°C, ruling out a thermal pathway (table S1, entries 2 and 3). The presence of air inhibited the reaction (table S1, entry 4). An increase in temperature enhanced the efficiency of the reaction, whereas a decrease in temperature diminished reaction efficiency (table S4). When the amount of water added to the reactants was reduced, the reaction could still be similarly accelerated (table S5). Implementation of the standard reaction under different micellar conditions resulted in a substantial decrease in product yield (table S6).

The absence of any additives in our reaction system implies that the formation of EDA complexes between reactants is essential in enabling the light-induced cross-coupling reactions. Therefore, the exploration of reactants with different electron affinities serves as the fundamental basis for investigating the substrate scope in cross-coupling reactions. Furthermore, the stability of reactants in the presence of water is a pivotal factor for the generation of the target products. Based on this, the scope of C(sp^2)–N bond formation was investigated (Fig. 3 and fig. S1). Indoles (**c1** to **c9**) underwent

Institute of Organic Chemistry, Faculty of Chemistry and Pharmacy, University of Regensburg, 93040 Regensburg, Germany.
*Corresponding author. Email: Burkhard.Koenig@chemie.uni-regensburg.de

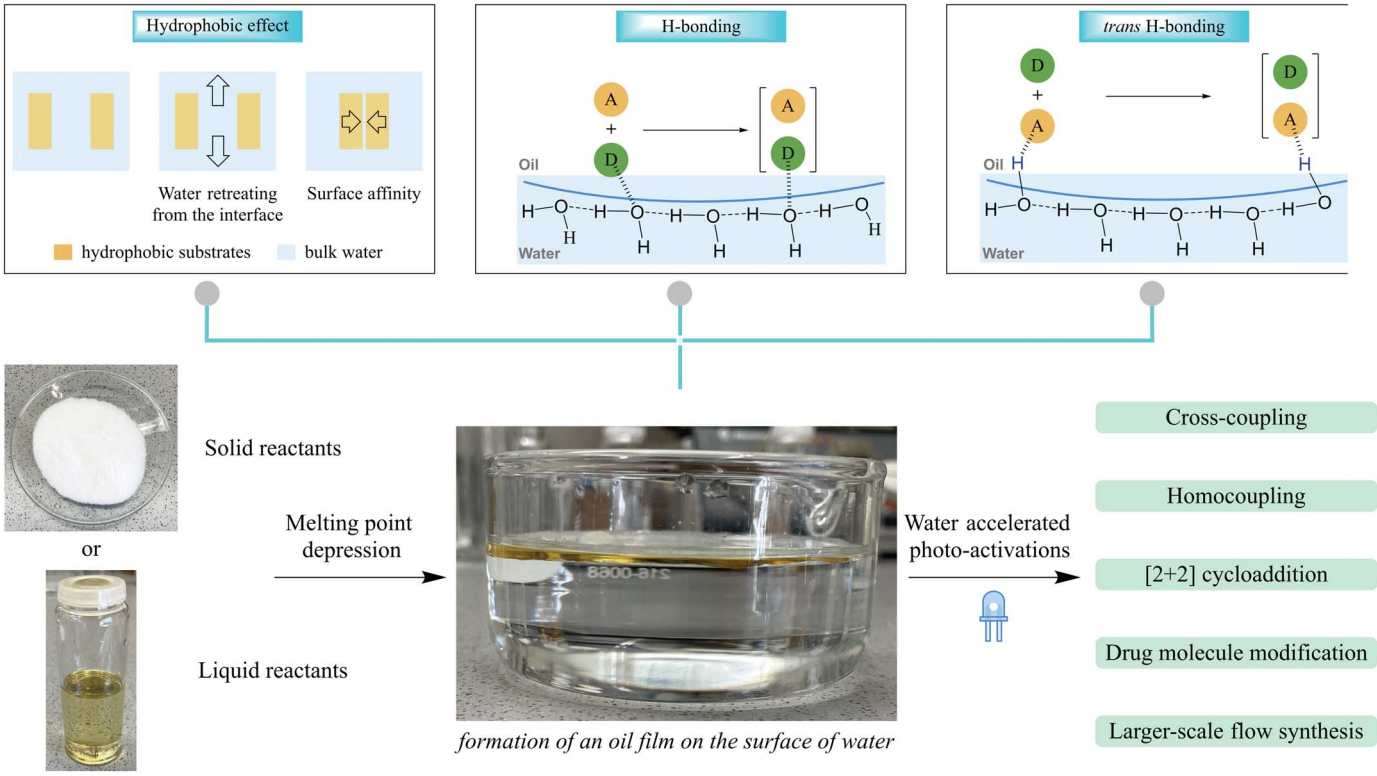

Fig. 1. Water-accelerated photochemical reactions. Water-accelerated photochemical reactions at the oil-water interface were successfully achieved without any additives, resulting in the transformations of cross-coupling, homocoupling, and [2+2] cycloaddition. This method was applied to the modification of drug molecules and gram-scale synthesis. "H-bonding" represents the H bonding formed between the active H of electron donor reactants and the oxygen atoms of water molecules. It is crucial for eliminating protons in the process of cross-coupling reactions. "*trans*-H-bonding" represents the H bonding formed between the electron acceptor reactants and the freely dangling H atoms at the aqueous interfacial layer. It is a potential driving force for the departure of leaving groups in the cross-coupling process.

successful conversion to the desired products. Furthermore, 1,2,3,4-tetrahydrocyclopentaindole proved capable of generating the arylation product **c10**. Various cyclic arylamines, including indolines (**c11** to **c15**) and hydroquinolines (**c16** to **c20**), were also compatible with the optimal conditions. This straightforward approach allowed for the direct C(sp^2)–N coupling of primary arylamines (**c21** to **c45**). Various substituted anilines (**c21** to **c43**) smoothly afforded the desired products, and naphthalen-2-amine (**c44**) and pyren-1-amine (**c45**) were readily accommodated. Secondary amines efficiently acted as N–H donors in the C–N coupling reactions (**c46** to **c58**). Electron-rich substrates (**c47** to **c49**) displayed efficient conversion. The presence of halogens (**c50** and **c51**) did not hinder the reaction. Different substituents on the N atom of aniline (**c52** to **c58**) successfully participated in the reactions. We also evaluated the performance of various heteroarylnitriles (**c59** to **c74**) in this protocol. Control experiments validated the successful extension of the protocol to activate C–F bonds (table S8).

The compatibility of this system with substrates bearing different leaving groups was subsequently verified. F, Cl, Br, and SO_2CH_3 exhibited excellent leaving group properties in constructing C(sp^2)–N bonds through reactions with various arylamines (**c75** to **c83**).

We next proceeded to validate the reactivity of a series of phenolic compounds (Fig. 4 and ig. S1) and were pleased to observe the successful formation of various C(sp^2)–O bonds (**c84** to **c91**). Both electron-donating and electron-withdrawing phenolic compounds were able to generate the desired products efficiently. Furthermore, this system exhibited compatibility with diverse heteroaryl substrates (**c91**).

We next explored phenylselenol compounds for cross-coupling reactions. The isoquinoline compound (**c92**), pyridine derivatives (**c93** and **c94**), and their pyrazine counterpart (**c95**) were effectively activated, facilitating the construction of distinct C(sp^2)–Se bonds. Subsequently, we successfully activated a range of arylthiols, enabling the construction of C(sp^2)–S bonds. Various substituents (**c96** to **c105**) afforded the corresponding products in good yields. Naphthylthiophenol (**c106**) and mercaptopyridine (**c107** and **c108**) also proved to be highly reactive substrates. Additionally, diverse heterocyclic substrates (**c109** to **c112**) were effectively incorporated into the reaction system.

We extended the reaction approach to the arylation of C(sp^3)–H bonds, enabling direct construction of C(sp^3)–C(sp^2) bonds, which is a challenging transformation in organic synthesis (*27*). Control experiments confirmed the photochemical nature of this reaction. Water substantially accelerated the reaction compared with other solvents (table S9). N-protected indoles (**c113** to **c122**), benzofurans (**c123** to **c125**), benzothiophenes (**c126** and **c127**), the α-amino compound (**c128**), and benzene derivatives (**c129** and **c130**) were smoothly converted in the C(sp^3)–C(sp^2) bond formation. Different cyano-substituted heteroarylnitriles were also compatible (**c131** to **c137**).

The antipsychotic drug intermediates iminodibenzyls (**c138** and **c139**), a depramine derivative (**c140**), antiviral drug intermediates (**c141** and **c142**), the anticonvulsant aminoglutethimide (**c143** to **c145**), the antibacterial sulfanilamide (**c146**), the local anesthetic benzocaine (**c147**), the anti-infective dapsone (**c148**), and the drug intermediate BAPS (**c149**) were successfully substituted with quinoline or other N-heterocycles, demonstrating the application potential of this water-based system in medicinal chemistry.

The successful implementation of a two-step consecutive reaction synthesis further enhances

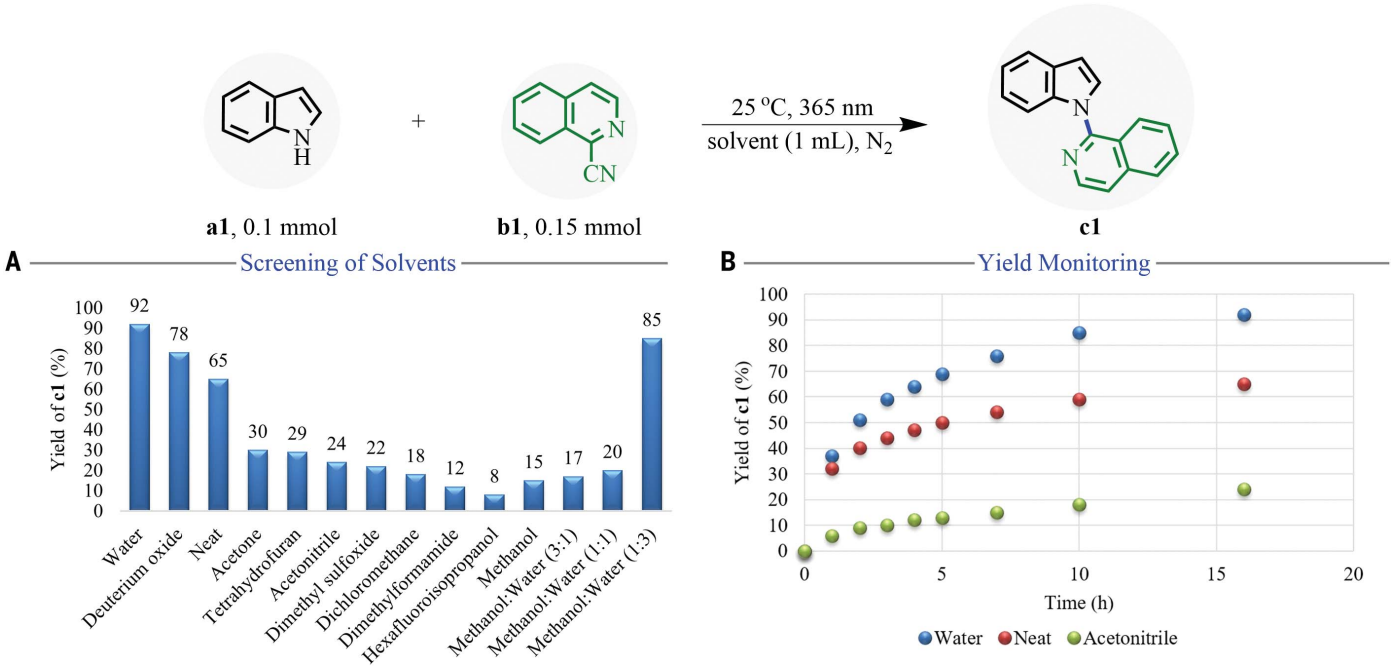

Fig. 2. Solvent screening for the standard reaction and monitoring of the overall yield under different conditions. (**A**) Water outperformed other organic solvents as a reaction medium, and its performance improved with higher proportions in mixtures with other solvents. (**B**) Water gave a higher overall reaction yield compared with neat conditions and acetonitrile. Product yield was monitored by GC-MS.

the practicality of this strategy (**c150** to **c157**). This application enables flexible switching between various aromatic heterocyclic substrates, achieving diverse aromatic functionalization with different reactive H substituents. Additionally, it enables convenient "one-pot" synthesis (**c150**).

Activating C(sp^3)–Cl bonds (**c158** to **c162**) extends the capability of this method, overcoming its restriction of exclusively activating C(sp^2)–Y bonds and thereby achieving the formation of C(sp^3)–C(sp^2) bonds.

Compared with organic solvents, water not only improved various photochemical cross-coupling reactions, but it also demonstrated a notable acceleration effect in a range of distinct photoreactions (tables S11 to S13), holding promise for broad application in homo-coupling reactions and [2+2] cycloadditions (**c163** to **c165**).

The quantum yield of the standard batch reaction was 4.6% (see the supplementary materials for details), and factors such as scattering in the reaction system contributed to this relatively low value. To address this practical issue, we developed a flow photochemical synthesis system and used it for the synthesis of product **c61** (Fig. 5A). To maximize interfacial area in the flow reactor, we used a segmented flow regime (*48*). This system enhances the interface through discrete liquid segments or droplets within an immiscible N_2 gas phase. These liquid segments, with elevated surface-to-volume ratios, facilitate intimate contact between aqueous and organic phases. The N_2 phase prevents coalescence, maintaining a distinct boundary and promoting efficient chemical transformations through enhanced intermolecular interactions (see the supplementary materials for details). We achieved the synthesis of 1.5 g of **c61** within 4 hours of reaction time, which showcases the potential for larger-scale synthesis using flow conditions in preparative water-interface photochemistry.

Mechanism

When the white solids **a1** and **b1** were combined in the presence of water, yellow oil droplets appeared (fig. S2). Melting point measurements indicated that stoichiometric mixtures of compound **a1** and **b1** form eutectic mixtures melting at room temperature, producing a yellowish oil (fig. S3). The presence of water may accelerate the diffusion of this oily substance on the surface. Ultraviolet-visible (UV-vis) spectroscopic analysis of this mixture showed a bathochromic shift of the longest wave absorption into the visible region of the spectrum (Fig. 5B), indicating the formation of an EDA complex between **a1** and **b1** (**EDA-1**).

Nuclear magnetic resonance (NMR) analysis was used to reveal the distribution of **a1**, **b1,** and **EDA-1** in the oily droplets and the water phase. To separately investigate the aqueous phase, the mixture was filtered, and the obtained clear, transparent, and colorless solution was investigated by NMR. The resulting ^{1}H spectrum (Fig. 5C and figs. S6 and S7) in D_2O exclusively showed signals of free **a1** and **b1** with deviating integrals (**a1**: **b1** = 7:1) caused by different solubilities. Next, this clear solution was irradiated (365 nm) for 2 hours, and no product **c1** was detected by gas chromatography–mass spectrometry (GC-MS). This result indicates that the microdispersed oily droplets in water are essential for a successful coupling reaction.

Next, the unfiltered microdispersion of **a1** and **b1** in D_2O was directly subjected to NMR. The resulting ^{1}H spectrum (Fig. 5D and fig. S8) showed contributions of both aqueous phase and oil droplets. The spectrum of this aqueous phase reproduced exactly the spectrum of the previously filtered aqueous phase and showed free **a1** and **b1** (Fig. 5, C and D). In addition, a new set of signals appeared in association with the oily droplets. A complete assignment revealed a 1:1 ratio of **a1** and **b1** in this complex, in which all signals of **a1** and **b1** were greatly shifted upfield by 0.53 to 1.83 ppm. These large shifts are typical for π/π complexes (*49*), and the bathochromic shift in the UV spectrum corroborates the formation of **EDA-1** in the oily droplets (Fig. 5).

Next, the interaction of **EDA-1** with water molecules was addressed. Because exchange with water does not allow for a direct detection of the indole N–H, the adjacent proton 2 was chosen as a sensor for the water interaction. Indeed, the one-dimensional (1D) nuclear Overhauser effect (NOESY) spectrum (Fig. 5E) revealed a small cross-peak between proton 2' of the indole moiety in **EDA-1** and water, which was not visible for proton 2 in free **a1** in the

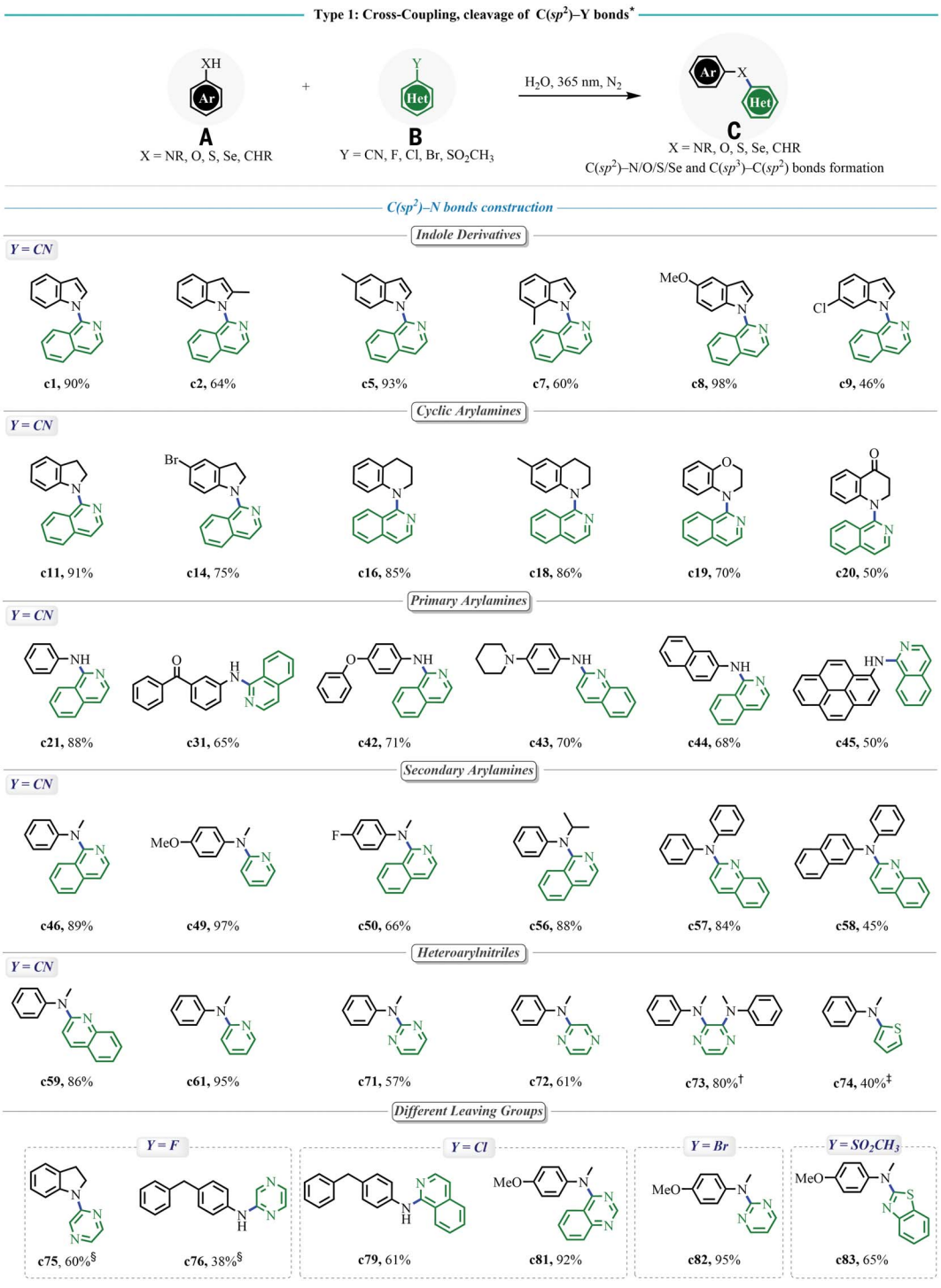

Fig. 3. Evaluation of substrate scope. *Isolation conditions: **a** (0.5 mmol), **b** (0.75 mmol) with 3 ml of water under 365 nm LED (3.0 W) light irradiation at 25°C under N_2 atmosphere for 16 hours. Reported yields are isolated yields. †1.0 mmol **a** and 0.5 mmol **b** were used. ‡Reaction time was 24 hours. §The reaction was conducted at 60°C for 48 hours.

aqueous phase (fig. S11). Considering the applied 9:1 ratio of D_2O to water and the remote position of proton 2, this indicates a prolonged lifetime of a water molecule near proton 2'. We attributed this to the formation of H bonding between the N–H of indole and water in the oily droplets. At this point, neither intermolecular NOE contacts between **a1** and **b1** within **EDA-1** nor in water solution were detected by 2D NOESY NMR (Fig. 5F and fig. S12). Instead, unexpectedly strong exchange cross-peaks, observed even at mixing times as low as 100 ms, linked free **a1**/**b1** in the water phase with **EDA-1** in the droplets [see "EXSY" (exchange signals) in Fig. 5E and, e.g., 8-8′ or 2-2′ in Fig. 5F]. These EXSYs in the NOESY spectra signify a very high mobility of **a1**/**b1** freely dispersed in solution and the analogous molecules within the **EDA-1**

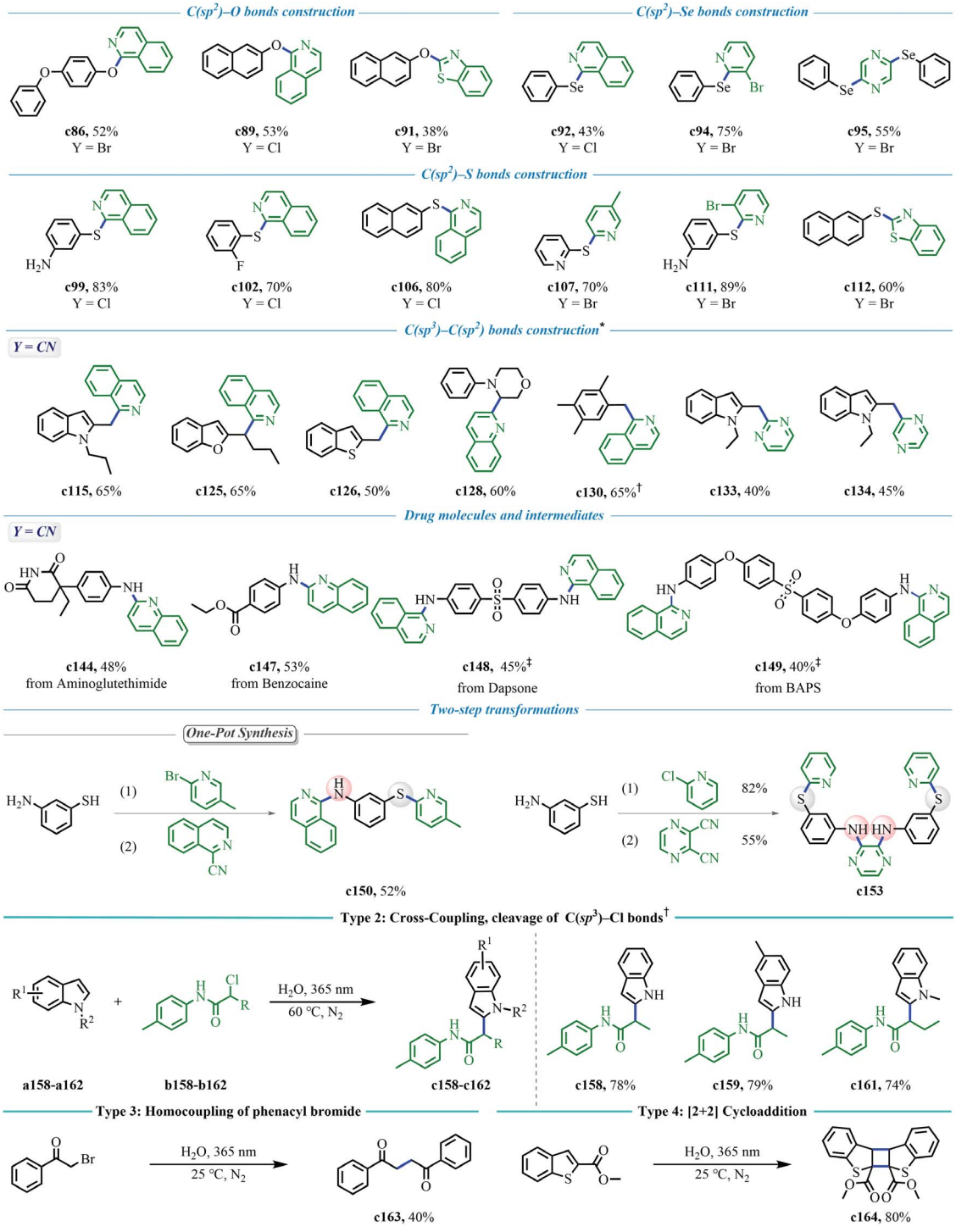

Fig. 4. Evaluation of substrate scope (continuation of Fig. 3). Isolation conditions: **a** (0.5 mmol), **b** (0.75 mmol) with 3 ml of water under 365 nm LED (3.0 W) light irradiation at 25°C under N_2 atmosphere for 16 hours. Reported yields are isolated yields. *Reaction time was 24 hours. †The reaction was conducted at 60°C for 16 hours. ‡1.25 mmol of **b** was used.

complex. The molecules can easily move between droplets and water. In addition, a dynamic light-scattering study (fig. S17) revealed an overall decreasing droplet size in the mixture of **a1** and **b1** after filtration over time. These results indicate an extremely fast exchange of the substrates between the two phases and corroborate the existence of **EDA-1** complexes directly at the droplet-water interphase. In addition, this low barrier of the interphase may explain the effective reaction and the high yields despite the phase separation. A recent study (*50*) used molecular dynamics simulations and heterodyne-detected vibrational sum frequency generation to confirm the formation of H bonds between the O–H group in phenol and water at the interface. This provides additional evidence to support our mechanistic investigations.

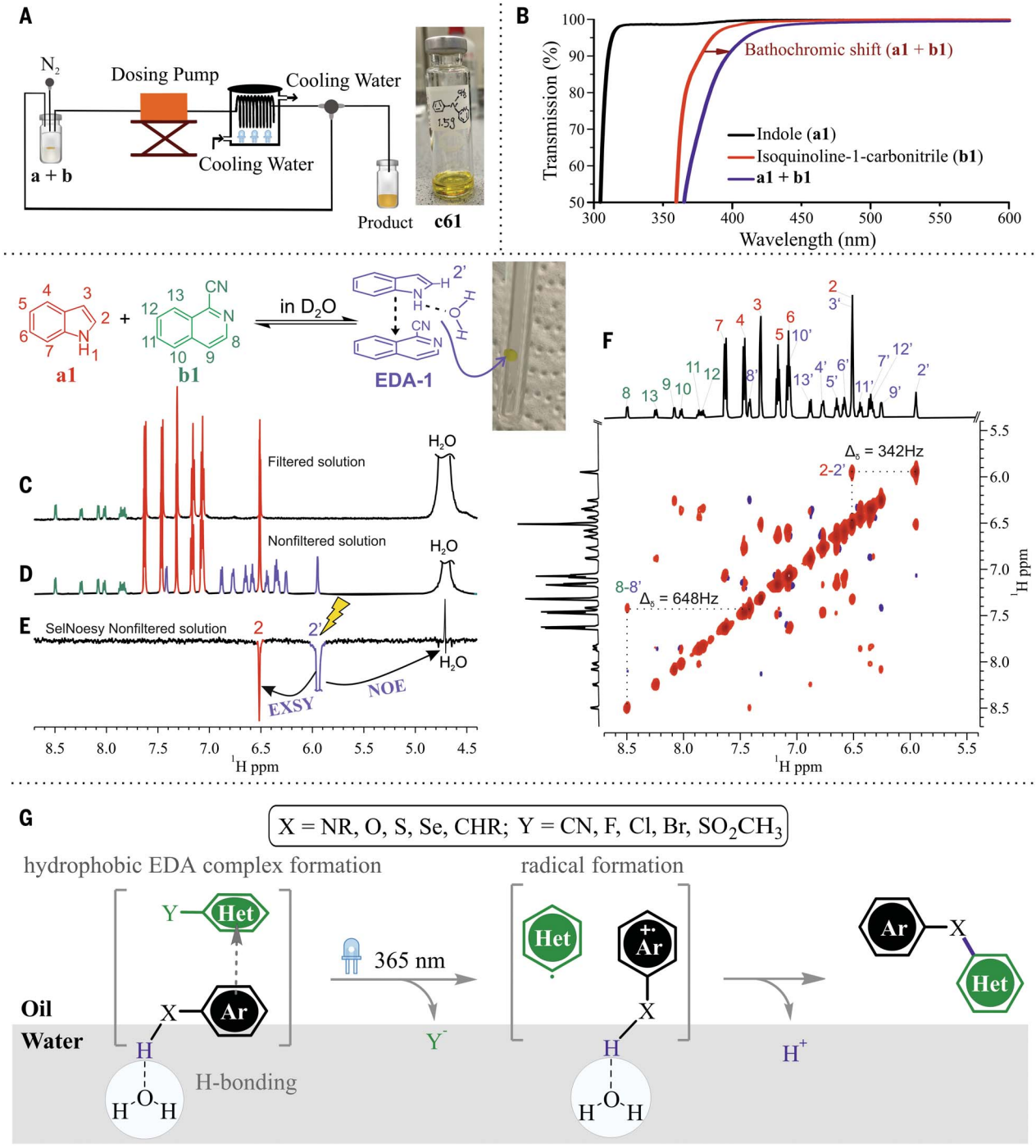

Fig. 5. Large-scale synthesis and mechanistic investigations. (**A**) A flow photoreactor enables efficient large-scale synthesis. (**B**) UV-vis absorption spectra of reaction components in methanol showed a new absorption band upon mixing **a1** and **b1**. [**a1**] = 0.03 M, [**b1**] = 0.03 M, **a1:b1** = 1:1. (**C**) ^{1}H NMR spectrum of the filtered mixture of a1 and b1 in D_2O, showing no evidence of EDA complex in the aqueous phase. (**D**) ^{1}H NMR spectrum of the nonfiltered mixture in D_2O exhibited an additional, upfield shifted set of signals, suggesting the formation of an EDA complex. (**E**) 1D NOESY experiment in D_2O at 298 K. Upon excitation of proton 2′ of EDA-1, a NOESY cross-peak to water was detected, indicating the contact between EDA-1 and water. (**F**) At 298 K, a 2D NOESY of a nonfiltered mixture in D_2O showed proton exchange between dissolved a1, b1, and EDA-1 at the D_2O interface. (**G**) Proposed mechanism.

Irradiation of the unfiltered sample in D_2O for 2 hours at 365 nm led to the formation of the desired product **c1** with a yield of 45%, as detected by GC-MS analysis. These findings conclusively confirm the formation of an EDA complex between **a1** and **b1** at the water interface, where the N–H group of the EDA complex interacts with water through H bonding, and the coupling reaction occurs upon light irradiation. Deuterium isotope effects indicate H bonding in organic reactions at the water interface (*4*). The reduced yield observed in D_2O, as compared with water, can be attributed to the reduced H-bond strength formed between the reactants and D_2O, leading to an increase

in the activation energy of the reaction and resulting in a lower yield (Fig. 2) upon replacement of water by D_2O.

Control experiments were conducted to investigate the hydrophobic effect (*13*–*17*) of water on the reaction system (table S15). The introduction of the prohydrophobic salt LiCl led to a moderate enhancement in the reaction efficiency. Conversely, the presence of the antihydrophobic agent guanidinium chloride resulted in a partial reduction of the reaction yield, indicating the importance of a certain degree of hydrophobicity in water, albeit with subtle effects.

GC-MS analysis of the crude photochemical reaction mixture of **a1** and **b1** detected the presence of HCN upon completion, and pH value monitoring (fig. S18) indicated a slight acidification of the water after the reaction (from pH ≈7 to pH ≈6), which resulted from HCN formation. The propensity for *trans*-H-bond formation (*4*), along with the fast equilibrium reaction involving cyanide anions and hydronium leading to the production of HCN and water, likely contributes to the effectiveness of cyanide anions as a leaving group in the presence of water. To mitigate the toxicity arising from HCN, a basic solution was used in the work-up process to react with HCN, forming less dangerous cyanide anions (see the supplementary materials for details).

Considering these investigations, a mechanism for the water-accelerated photoinduced reactions is proposed (Fig. 5G). Initially, melting point depression occurs upon mixing the reactants, and the hydrophobic effect of water forces the two reactants to form an EDA complex on the water surface, creating an oil-water interface, where the reactive H atoms in the reactants form H bonds with water. This process accelerates the single-electron transfer under light irradiation, leading to the formation of radical ion pairs, which subsequently generate radicals and ultimately yield the coupling product, simultaneously eliminating an anion and a proton. Essential is the very fast exchange between the water-dissolved molecules and the oil-phase molecules observed by NMR measurements because this allows the conversion of all starting materials into the desired products.

Conclusions

We have developed a new photochemical reaction mode that involves mixing water-insoluble reactants with different electron affinities, including solid compounds. When these reactants interact, they form EDA complexes, and the resulting melting point depression creates, in conjunction with water, an H-bond–connected, eutectic oil-water interface. Under light irradiation, a series of accelerated cross-coupling reactions occur. Additionally, we have used the accelerating effect of water on photoinduced homocoupling reactions and [2+2] cycloaddition reactions. Our experiments show that photochemical reactions at the water interface provide opportunities to enhance chemical synthesis. The methodology is well suited for drug molecule modification for continuous reactions and flow conditions, enabling diversifying the functionalization of molecules and facilitating their efficient larger-scale synthesis. The reported simple reaction conditions avoid any toxic or flammable solvent or additives and improve and facilitate chemical transformations in and beyond chemistry or in industrial processes for which the highest efficiency is in demand.

REFERENCES AND NOTES

1. D. C. Rideout, R. Breslow, *J. Am. Chem. Soc.* **102**, 7816–7817 (1980).
2. C.-J. Li, *Chem. Rev.* **93**, 2023–2035 (1993).
3. R. N. Butler, A. G. Coyne, *Chem. Rev.* **110**, 6302–6337 (2010).
4. M. Cortes-Clerget *et al*., *Chem. Sci.* **12**, 4237–4266 (2021).
5. T. Kitanosono, S. Kobayashi, *Chemistry* **26**, 9408–9429 (2020).
6. C. Jimeno, *Org. Biomol. Chem.* **14**, 6147–6164 (2016).
7. T. Kitanosono, K. Masuda, P. Xu, S. Kobayashi, *Chem. Rev.* **118**, 679–746 (2018).
8. B. H. Lipshutz, S. Ghorai, M. Cortes-Clerget, *Chemistry* **24**, 6672–6695 (2018).
9. A. Manna, A. Kumar, *J. Phys. Chem. A* **117**, 2446–2454 (2013).
10. D. B. Eremin, V. V. Fokin, *J. Am. Chem. Soc.* **143**, 18374–18379 (2021).
11. S. Narayan *et al*., *Angew. Chem. Int. Ed.* **44**, 3275–3279 (2005).
12. Y. Jung, R. A. Marcus, *J. Am. Chem. Soc.* **129**, 5492–5502 (2007).
13. R. Breslow, R. Connors, Z. Zhu, *Pure Appl. Chem.* **68**, 1527–1533 (1996).
14. R. Breslow, K. Groves, M. U. Mayer, *Pure Appl. Chem.* **70**, 1933–1938 (1998).
15. R. Breslow, *Acc. Chem. Res.* **24**, 159–164 (1991).
16. R. Breslow, C. J. Rizzo, *J. Am. Chem. Soc.* **113**, 4340–4341 (1991).
17. R. Breslow, K. Groves, M. U. Mayer, *J. Am. Chem. Soc.* **124**, 3622–3635 (2002).
18. L. F. Scatena, M. G. Brown, G. L. Richmond, *Science* **292**, 908–912 (2001).
19. A. A. Bakulin *et al*., *Acc. Chem. Res.* **42**, 1229–1238 (2009).
20. S. Otto, J. B. F. N. Engberts, *Org. Biomol. Chem.* **1**, 2809–2820 (2003).
21. Y. R. Shen, V. Ostroverkhov, *Chem. Rev.* **106**, 1140–1154 (2006).
22. Q. Du, E. Freysz, Y. R. Shen, *Science* **264**, 826–828 (1994).
23. C. Russo, F. Brunelli, G. C. Tron, M. Giustiniano, *J. Org. Chem.* **88**, 6284–6293 (2023).
24. C. Zhou *et al*., *J. Am. Chem. Soc.* **142**, 16805–16813 (2020).
25. C. Zhou *et al*., *Angew. Chem. Int. Ed.* **61**, e202116421 (2022).
26. A. McNally, C. K. Prier, D. W. C. MacMillan, *Science* **334**, 1114–1117 (2011).
27. J. D. Cuthbertson, D. W. C. MacMillan, *Nature* **519**, 74–77 (2015).
28. X. Hui *et al*., *Green Chem.* **25**, 2274–2278 (2023).
29. V. Jeyapalan, R. Varadharajan, G. B. Veerakanellore, V. Ramamurthy, *J. Photochem. Photobiol. Chem.* **420**, 113492–113501 (2021).
30. M. S. Syamala, V. Ramamurthy, *J. Org. Chem.* **51**, 3712–3715 (1986).
31. N. A. Stini *et al*., *Org. Biomol. Chem.* **21**, 1284–1293 (2023).
32. J. C. G. Kürschner, L. Brüss, L. Naesborg, *Chemistry* **29**, e202300627 (2023).
33. C. J. C. Jordan, E. A. Lowe, J. R. R. Verlet, *J. Am. Chem. Soc.* **144**, 14012–14015 (2022).
34. M. T. C. Martins-Costa, J. M. Anglada, J. S. Francisco, M. F. Ruiz-López, *Chem. Sci.* **13**, 2624–2631 (2022).
35. R. Schulte, M. Löcker, H. Ihmels, M. Heide, C. Engelhard, *Chemistry* **29**, e202203203 (2023).
36. K. J. Kappes *et al*., *J. Phys. Chem. A* **125**, 1036–1049 (2021).
37. R. Naumann, M. Goez, *Green Chem.* **21**, 4470–4474 (2019).
38. E. Speckmeier, P. J. W. Fuchs, K. Zeitler, *Chem. Sci.* **9**, 7096–7103 (2018).
39. D. Xue *et al*., *Chemistry* **20**, 2960–2965 (2014).
40. P. Natarajan, D. Chuskit, Priya, *Green Chem.* **21**, 4406–4411 (2019).
41. J. Lu *et al*., *Adv. Synth. Catal.* **362**, 2178–2182 (2020).
42. S. Pan *et al*., *Green Chem.* **22**, 336–341 (2020).
43. G. F. P. de Souza, J. A. Bonacin, A. G. Salles Jr., *J. Org. Chem.* **83**, 8331–8340 (2018).
44. R. C. W. van Lier, A. D. de Bruijn, G. Roelfes, *Chemistry* **27**, 1430–1437 (2021).
45. S. Srinath *et al*., *Green Chem.* **22**, 2575–2587 (2020).
46. G. E. M. Crisenza, D. Mazzarella, P. Melchiorre, *J. Am. Chem. Soc.* **142**, 5461–5476 (2020).
47. A. K. Wortman, C. R. J. Stephenson, *Chem* **9**, 2390–2415 (2023).
48. N. Weeranoppanant, *React. Chem. Eng.* **4**, 235–243 (2019).
49. A. S. Shetty, J. Zhang, J. S. Moore, *J. Am. Chem. Soc.* **118**, 1019–1027 (1996).
50. R. Kusaka, T. Ishiyama, S. Nihonyanagi, A. Morita, T. Tahara, *Phys. Chem. Chem. Phys.* **20**, 3002–3009 (2018).

ACKNOWLEDGMENTS

We thank R. Vasold for the assistance in GC-MS measurements, J. Zach for the technical assistance, and H. Motschmann and W. Kunz for discussions and advice. **Funding:** This work was supported by the Deutsche Forschungsgemeinschaft [DFG (German Science Foundation) grant TRR 325-444632635]. W.S. is funded by DFG grant RTG 2620, "Ion Pair Effects in Molecular Reactivity," project 426795949). **Author contributions:** Y.-M.T. and B.K. conceived the project. Y.-M.T. performed and analyzed the experiments. W.S. performed the in situ NMR experiments for the investigations of the mechanism under the supervision of R.M.G. Y.-M.T. and B.K. wrote the manuscript with input from all authors. All authors discussed the results. **Competing interests:** The authors declare no competing interests. **Data and materials availability:** All data are available in the main text or the supplementary materials.

SUPPLEMENTARY MATERIALS

science.org/doi/10.1126/science.adl3092
Materials and Methods
Supplementary Text
Figs. S1 to S18
Tables S1 to S15
References (*51*–*95*)

Submitted 11 October 2023; accepted 11 January 2024
10.1126/science.adl3092